Additive-Mediated Crystallization of Complex Calcium Carbonate Superstructures in Reverse Microemulsions

Surachai Thachepan, Mei Li, Sean A. Davis, and Stephen Mann*

Centre for Organized Matter Chemistry, School of Chemistry, University of Bristol, Bristol BS8 1TS, United Kingdom

Received April 12, 2006. Revised Manuscript Received May 10, 2006

Morphologically complex forms of calcium carbonate were produced within 24 h in unstirred mixtures of $Ca(AOT)_2$ (AOT = bis(2-ethylhexyl)sulfosuccinate) reverse micelles and carbonate-containing NaAOT microemulsions ($w = 10$). The structures form by controlled aggregation of surfactant-coated amorphous calcium carbonate primary particles, which resulted in micrometer-sized doughnut-shaped structures consisting of densely packed layers of platelike aragonite crystals. These superstructures were progressively in-filled to produce polycrystalline multilayered spindle-shaped particles several micrometers in length. Addition of the crystallization additive sodium polyphosphate at concentrations exceeding 1 g L^{-1} to the carbonate-containing NaAOT microemulsions inhibited aragonite crystallization, with the consequence that single crystals of calcite with bundlelike filamentous texture along with platelike vaterite single crystals were produced. Energy-dispersive X-ray analysis indicated that AOT and polyphosphate ions were strongly associated with the crystals even after extensive washing. Unlike the aragonite superstructures, which became decorated within a few days with epitaxially oriented rodlike outgrowths of calcite, the platelike vaterite and filamentous calcite crystals remained unchanged even after 7 days. The results demonstrate that encapsulation of crystallization additives such as polyphosphate in the water droplets of reverse microemulsions can be used to influence nucleation and growth processes over a range of length scales and suggest that this novel approach could be of interest in crystal science in general.

Introduction

The spontaneous assembly and transformation of nanosized building units into higher-order superstructures is a key challenge in the development of bottom-up approaches to integrated systems and devices at the nano/micro-interface.[1,2] While there are several well-established methods now available for nanoparticle assembly, notably, those involving interparticle DNA base pairing,[3] solvent evaporation,[4] hydrophobic interdigitation,[5] dipole−dipole propagation,[6] and inorganic,[7] organic,[8] or biological[9] templates, there are fewer reports on the use of nanoparticle-based transformations as routes to the spontaneous formation of higher-order architectures. These transformations often involve the complex interplay between crystallization and aggregation,[1] both of which are highly sensitive to changes in the local environment, with the consequence that the systems exhibit time- and scale-dependent structures and morphologies. Typically, nucleation and growth of the crystalline nanostructures occur within aggregates of amorphous inorganic particles that are partially stabilized by surface-adsorbed polymers/block copolymers (see ref 10 for an extensive overview) or surfactant molecules.[11] Because the crystallization process is strongly influenced by the collective properties of the colloidal aggregates, the transformations occur initially on the mesoscale, and small changes in the conditions can have a marked influence on the emergent behavior of the systems. This often results in a series of structural and morphological reorganizations that are length scale dependent. For example, studies on the crystallization of $CaCO_3$ in water-in-isooctane reverse microemulsions prepared from the surfactant, NaAOT

* To whom correspondence should be addressed. E-mail: s.mann@bris.ac.uk.

(1) Colfen, H.; Mann, S. *Angew. Chem., Int. Ed.* **2003**, *42*, 2350.
(2) Zeng, H. C. *J. Mater. Chem.* **2006**, *16*, 649−662.
(3) (a) Mirkin, C. A.; Letsinger, R. L.; Mucic, R. C.; Storhoff, J. J. *Nature* **1996**, *382*, 607−609. (b) Mirkin, C. A. *Inorg. Chem.* **2000**, *39*, 2258−2272. (c) Li, M.; Mann, S. *J. Mater. Chem.* **2004**, *14*, 2260−2263. (d) Sadasivan, S.; Dujardin, E.; Li, M.; Johnson, C. J.; Mann, S. *Small* **2005**, *1*, 103−106.
(4) (a) Murray, C. B.; Kagan, C. R.; Bawendi, M. G. *Science* **1995**, *270*, 1335−1338. (b) Wang, Z. L. *Adv. Mater.* **1998**, *10*, 13−30.
(5) Li, M.; Schnablegger, H.; Mann, S. *Nature* **1999**, 393−395.
(6) (a) Tlusty, T.; Safran, S. A. *Science* **2000**, *290*, 1328−1331. (b) Tang, Z. Y.; Kotov, N. A.; Giersig, M. *Science* **2002**, *297*, 237−240. (c) Lin, S.; Li, M.; Dujardin, E.; Girard, C.; Mann, S. *Adv. Mater.* **2005**, *17*, 2553.
(7) (a) Nagle, L.; Ryan, D.; Cobbe, S.; Fitzmaurice, D. *Nano Lett.* **2003**, *3*, 51−53. (b) Moghaddam, M. J.; Taylor, S.; Gao, M.; Huang, S. M.; Dai, L. M.; McCall, M. J. *Nano Lett.* **2004**, *4*, 89−93.
(8) (a) Burkett, S. L.; Mann, S. *Chem. Commun.* **1996**, 321−322. (b) Bae, A. H.; Numata, M.; Hasegawa, T.; Li, C.; Kaneko, K.; Sakurai, K.; Shinkai, S. *Angew. Chem., Int. Ed.* **2005**, *44*, 2030−2033. (c) Scheibel, T.; Parthasarathy, R.; Sawicki, G.; Lin, X. M.; Jaeger, H.; Lindquist, S. L. *Proc. Natl. Acad. Sci. U.S.A.* **2003**, *100*, 4527−4532.
(9) (a) Keren, K.; Krueger, M.; Gilad, R.; Ben-Yoseph, G.; Sivan, U.; Braun, E. *Science* **2002**, *297*, 72−75. (b) Warner, M. G.; Hutchison, J. E. *Nat. Mater.* **2003**, *2*, 272−277. (c) Behrens, S.; Rahn, K.; Habicht, W.; Bohm, K. J.; Rosner, H.; Dinjus, E.; Unger, E. *Adv. Mater.* **2002**, *14*, 1621−1625. (d) Dujardin, E.; Peet, C.; Stubbs, G.; Culver, J. N.; Mann, S. *Nano Lett.* **2003**, *3*, 413−417.
(10) Yu, S. H.; Colfen, H. *J. Mater. Chem.* **2004**, *14*, 2124.
(11) (a) Li, M.; Mann, S. *Langmuir* **2000**, *16*, 7088−7094. (b) Qi, L.; Ma, J.; Cheng, H.; Zhao, Z. *J. Phys. Chem.* **1997**, *101*, 3460. (c) Johnson, C. J.; Li, M.; Mann, S. *Adv. Funct. Mater.* **2004**, *14*, 1233. (d) Sadasivan, S.; Khushalani, D.; Mann, S. *Chem. Mater.* **2005**, *17*, 2765−2770.

10.1021/cm060847f CCC: $33.50 © 2006 American Chemical Society
Published on Web 06/17/2006

(sodium bis(2-ethylhexyl)sulfosuccinate), have reported a range of organized superstructures, such as vaterite nanoparticle/nanofilament arrays,[12] mesoporous aragonite nanofilament networks,[13] and stacked calcite lamellae,[14] depending on the $[H_2O]/[NaAOT]$ molar ratio ($w = 10$, 20, or 40, respectively) and number ratio of water droplets to amorphous $CaCO_3$ nanoparticles. The results suggested that the nanoparticle-based transformations were strongly modified by the degree of hydration at the surfactant−inorganic interface, which influenced the competition between formation of surfactant-stabilized aggregates and destabilization of the colloidal structures by water-induced crystallization.

In this paper, we investigate a new approach involving the encapsulation of a soluble crystallization inhibitor (sodium polyphosphate) into the water droplets of a reverse microemulsion prepared by mixing sodium carbonate-containing NaAOT microemulsions ($w = 10$) with an isooctane suspension of $Ca(AOT)_2$ reverse micelles. Sodium polyphosphate consists of a range of condensed chain polyphosphates and is a well-known corrosion and scale inhibitor and water softening and dispersing agent.[15] By incorporating this polyanion into the microemulsion water droplets we not only add a further level of complexity to the emergent system but also highlight an approach that may have relevance for the use of crystallization inhibitors in oil/water systems in general. Our results demonstrate that encapsulation of polyphosphate ions in the water droplets significantly influences the nucleation, growth, and morphology of calcium carbonate. Whereas micrometer-sized doughnut-shaped aragonite superstructures are produced in the absence of polyphosphate, entrapment of the polyanion at appropriate concentrations inhibits aragonite crystallization and promotes the formation of mixtures of filamentous calcite and plate-shaped vaterite single crystals. Furthermore, the aragonite superstructures become decorated within a few days with oriented rodlike outgrowths of calcite, while the filamentous calcite and platelike vaterite crystals remain unchanged even after 7 days.

Experimental Section

Analytical grade sodium carbonate anhydrous (Na_2CO_3) and NaAOT, calcium nitrate tetrahydrate and polyphosphate (sodium heptaphosphate; typical compositional range, $Na_{15}P_{13}O_{40}$ to $Na_{20}P_{18}O_{55}$), and isooctane (2,2,4-trimethylpentane) were purchased from BDH, Sigma, and Aldrich, respectively. All chemicals were used without any further purification. Calcium bis(2-ethylhexyl)-sulfosuccinate ($Ca(AOT)_2$) was synthesized according to the literature.[16]

Crystallization of $CaCO_3$ in microemulsion water droplets in the presence or absence of sodium polyphosphate was studied as follows. Water-in-oil microemulsions were prepared from aqueous Na_2CO_3 (0.1 M; pH = 8.7) at $w = 10$ by adding 270 μL of Na_2CO_3 solution to 15 mL of 0.1 M NaAOT in isooctane, followed by sonication in a water bath for 3 min. Coprecipitation of $CaCO_3$ was induced by adding 540 μL of 0.05 M $Ca(AOT)_2$ in isooctane to 15 mL of the carbonate-containing microemulsions, followed by vigorously shaking. The mixture was left to stand at room temperature for up to 1 week. Experiments were also undertaken under the same conditions but using sodium polyphosphate/carbonate-containing microemulsions and $Ca(AOT)_2$ reverse micelles. The former were prepared by adding various amounts of 10 g L^{-1} polyphosphate solution to aqueous Na_2CO_3 at pH = 8.7 (final concentrations, Na_2CO_3, 0.1 M; polyphosphate, 0.1, 0.5, 1.0, and 2.0 g L^{-1}).

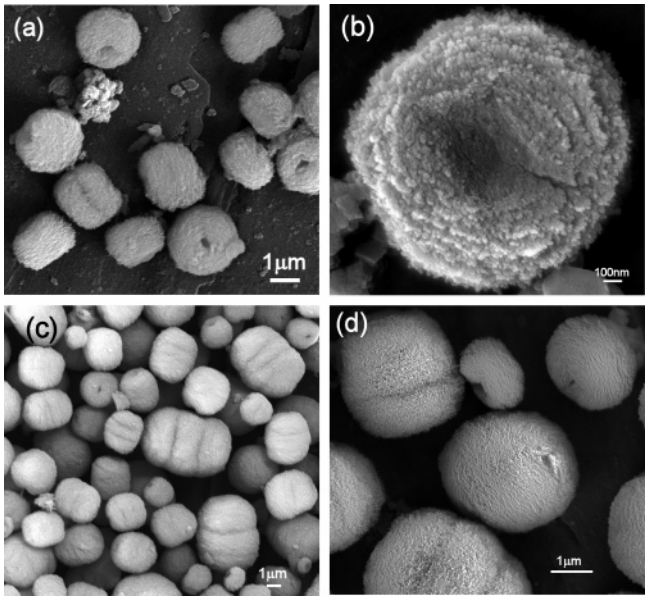

Figure 1. SEM images of calcium carbonate (aragonite) particles produced in microemulsions collected after (a) 2 h, showing doughnut-shaped crystals, (b) 3 h, showing a high magnification image of individual particle viewed along the radial axis, (c) 8 h, showing spindle-shaped crystals, and (d) 8 h, a high magnification image.

Samples were collected between 30 min and 1 week after mixing of the reagents, and in most cases excess surfactant was removed by washing and centrifugation with isooctane. Samples for transmission electron microscopy (TEM; JEOL 1200 EX, 120 keV), electron diffraction, and energy-dispersive X-ray (EDX) analysis were deposited on carbon-coated, 3 mm diameter, copper electron microscope grids. After drying in air, the grids were washed with pure isooctane. Samples for scanning electron microscopy (SEM, JEOL JSM 6330FEG, 1−30 keV) were mounted directly onto circular aluminum stubs, air-dried, and coated with a 15 nm thick Pd/Pt (AGAR high-resolution sputter-coater) or left uncoated. Materials for powder X-ray diffraction (PXRD) analysis were deposited on a silicon wafer sample holder and characterized using a Bruker D8 advanced diffractometer (Cu $K\alpha_1$ 1.5418 Å). Samples were studied by Fourier transform infrared (FTIR) spectroscopy using KBr disks.

Results and Discussion

In the absence of polyphosphate, addition of reverse micelles of $Ca(AOT)_2$ to water-in-oil carbonate-containing NaAOT microemulsions at $w = 10$ produced a transparent solution that became slightly opaque within 2 h, followed by the gradual appearance of a white precipitate. SEM images of samples collected from unstirred microemulsions after 2 h consisted exclusively of monodisperse doughnut-shaped particles of mean diameter 2.3 μm ($\sigma = 0.2$; Figure 1a). The high uniformity in particle size was consistent with a restricted nucleation stage followed by a period of slow

(12) Li, M.; Mann, S. *Adv. Funct. Mater.* **2002**, *12*, 773.
(13) Li, M.; Lebeau, B.; Mann, S. *Adv. Mater.* **2003**, *15*, 2032.
(14) Viravaidya, C.; Li, M.; Mann, S. *Chem. Commun.* **2004**, 2182−2183.
(15) (a) Papo, A.; Piani, L.; Ricceri, R. *Silic. Ind.* **2003**, *68*, 119. (b) Boffardi, B. P. *Mater. Perform.* **1993**, *32*, 50.
(16) Eastoe, J.; Fragneto, G.; Robinson, B. H.; Towey, T. F.; Heenan, R. K.; Leng, F. J. *J. Chem. Soc., Faraday Trans.* **1992**, *88*, 461.

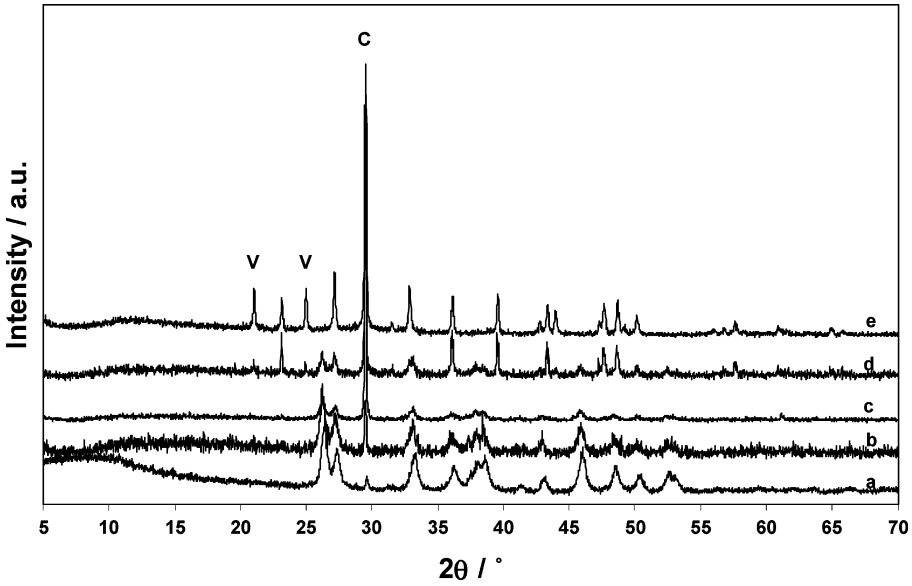

Figure 2. PXRD profiles of calcium carbonate samples collected after 24 h (a) in the absence of polyphosphate (aragonite); (b−e) in the presence of polyphosphate at different concentrations; (b) 0.1 g L^{-1} (aragonite + calcite), (c) 0.5 g L^{-1} (aragonite + calcite), (d) 1.0 g L^{-1} (calcite + aragonite), and (e) 2.0 g L^{-1} (calcite + vaterite). (Peak marked C corresponds to the calcite {104} reflection; peaks marked V correspond to vaterite {002} and {100} reflections).

growth. Each particle comprised overlapping layers of platelike crystals arranged at progressively decreasing angles to the radial morphological axis (Figure 1b). Addition of further layers resulted in in-filling of the doughnut-like morphology to produce spheroidal structures (mean size, 2.8 μm ($\sigma = 0.3$)), which subsequently developed into highly textured spindle-shaped crystals (mean length and width, 3.6 μm ($\sigma = 1.0$) and 3.0 μm ($\sigma = 0.7$)) at around 4 and 8 h, respectively (Figure 1c,d). Closure of the structures appeared to be self-limiting such that the rate of growth was significantly curtailed, and as a consequence a second generation of doughnut-shaped particles was produced in the reaction solution at times beyond 6 h. Thus, samples collected after 6 h typically consisted of mixtures of the two morphological forms; for example, both doughnut-shaped (mean size, 1.1 μm ($\sigma = 0.6$) and spindle-shaped particles (mean width and length, 4.0 μm ($\sigma = 0.2$) and 5.2 μm ($\sigma = 0.2$), respectively) were obtained in materials collected after 24 h.

PXRD analysis of the above samples showed sharp reflections consistent with the aragonite polymorph of calcium carbonate (*d* spacings/nm (*hkl*): 0.338 (111), 0.326 (021), 0.269 (012), 0.248 (200), 0.236 (112), 0.233 (130), 0.210 (220), 0.197 (221), 0.187 (202), 0.181 (132), 0.174 (113), and 0.173 (231)), as well as a broad peak at $2\theta = 10°$ corresponding to amorphous calcium carbonate[17] (Figure 2a). The presence of aragonite was confirmed by FTIR spectroscopy, which showed characteristic absorption bands at 700, 712, 860, 1082, and 1476 cm^{-1}. In addition, FTIR spectra of washed samples showed bands corresponding to organic functional groups, such as ester C═O (1735 cm^{-1}), ester C═O and S═O (1218 cm^{-1}), CH methyl (2961, 2871 cm^{-1}), and CH methylene (2924, 2858 cm^{-1}) absorbances, indicating that surfactant molecules were strongly associated with the aragonite superstructures.

TEM images of samples collected after 30 min showed discrete electron dense particles less than 10 nm in size (Figure 3a), along with loosely packed nanoparticle-containing aggregates of mean dimension, 475 nm ($\sigma = 37$; Figure 3b). EDX analysis of individual aggregates showed peaks for Ca (3.7, 4.0 keV), S (2.3 keV), and Na (1.0 keV), and no reflections were observed by electron diffraction, suggesting that the clusters consisted of surfactant-coated amorphous $CaCO_3$ nanoparticles. In contrast, aggregates collected after 1 h showed a distinct doughnut-like morphology (Figure 3c), and corresponding electron diffraction analysis gave pseudo-single crystal patterns that showed a

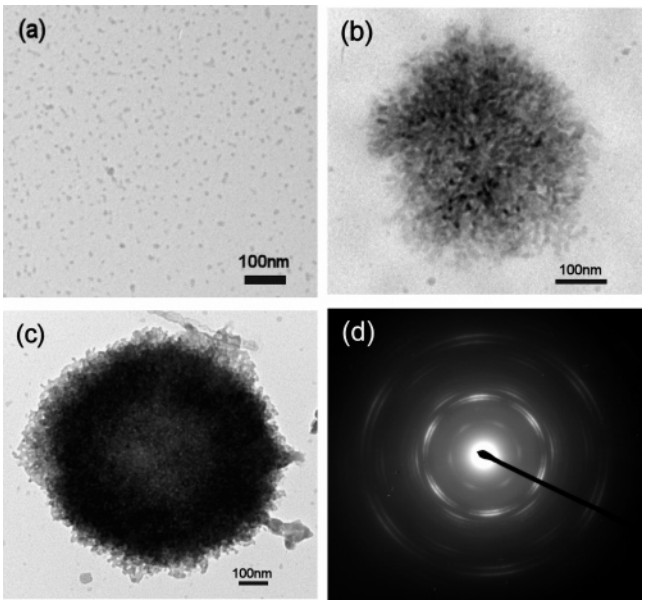

Figure 3. TEM images showing early stages of growth of aragonitic superstructures. Samples collected after (a) 30 min, showing discrete electron dense amorphous nanoparticles, (b) 30 min, showing single aggregate consisting of loosely packed amorphous nanoparticles, (c) 1 h, showing aggregate with doughnut-like projection, and (d) 1 h, showing powder electron diffraction from individual aggregates with strong arced *d* spacings at (*hkl*) indices corresponding to (110), (020), (200), (210), (220), (040), (330), (060), (400), and (420) planes.

(17) Aizenberg, J.; Lambert, G.; Addadi, L.; Weiner, S. *Adv. Mater.* **1996**, *8*, 222.

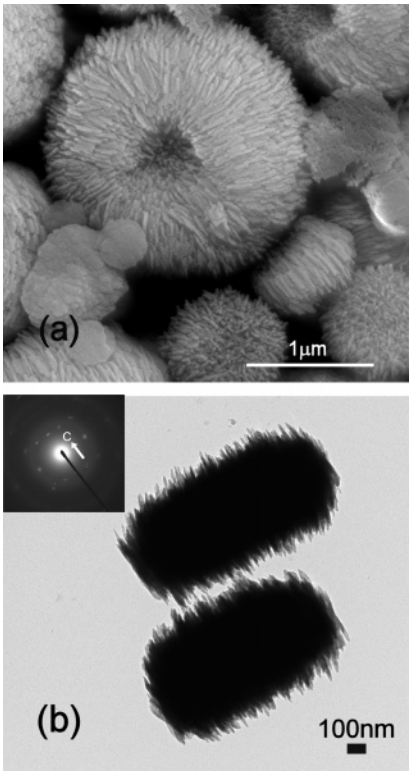

Figure 4. (a) SEM image showing oriented calcitic overgrowth of doughnut-shaped aragonite particles after 7 days. (b) TEM image showing side view of doughnut shaped particles and elongated calcitic outgrowths parallel to the morphological radial axis. Inset shows corresponding electron diffraction pattern from the particle in the upper part of the TEM image. The pattern corresponds to the $\{1\bar{1}0\}$ zone of calcite and indicates that the direction of calcitic outgrowth is aligned parallel to the [001] crystallographic axis.

series of arced reflections that were consistent with a view along the [001] zone of aragonite (Figure 3d). Thus, the crystalline aggregates were highly textured aragonite single crystals or, alternatively, polycrystalline structures with a high degree of preferred orientation. The results indicated that formation of the initial stage of the doughnut-shaped aragonite superstructure occurred through the transformation of aggregates of surfactant-coated amorphous nanoparticles and that this process involved coherent crystallization within the colloidal phase rather than primary nucleation from solution.

Interestingly, increasing the reaction times beyond 1 day resulted in extensive transformation of the surface texture of the spindle- and doughnut-shaped particles. With time, the stacked platelike arrangement aligned normal to the long/radial axis of these particles was replaced with a striated pattern of rodlike outgrowths that were oriented parallel to this morphological direction (Figure 4a). PXRD analyses of precipitates collected after 7 days showed no change in the relative intensities of the aragonite peaks observed for samples after 1 day, but a significant reduction in the intensity of the amorphous calcium carbonate broad band at $2\theta = 10°$ and the presence of an additional high intensity reflection corresponding to the {104} refection of calcite ($d = 0.303$ nm) were observed (data not shown). Optical Raman microscopy analysis of single particles also confirmed the presence of calcite. TEM and electron diffraction studies confirmed that the aged material consisted of spindle- and doughnut-shaped aragonite particles decorated with outgrowths of calcite nanofilaments oriented along the crystallographic [001] axis and lying parallel to the morphological long/radial axis of the particles (Figure 4b). The 90° change in surface texture was consistent with epitaxial nucleation of the calcite (001) face on exposed areas of the underlying aragonite (001) plates, presumably as a result of a high degree of lattice matching between the relative positions of Ca^{2+} ions in these faces. As epitaxial growth generally requires low supersaturation levels in the crystallization solution, one possibility is that this is achieved in the microemulsions by the dissolution of extraneous amorphous calcium carbonate particles present in the reaction medium.

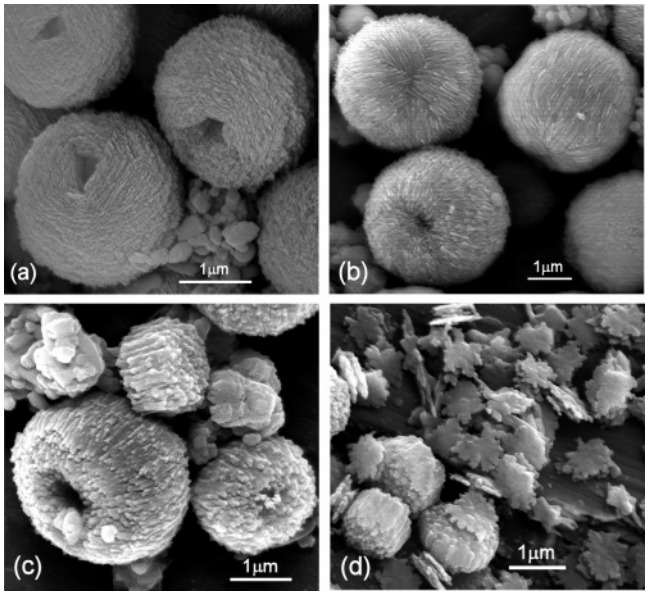

Figure 5. SEM images of calcium carbonate particles produced in microemulsions in the presence of sodium polyphosphate: (a) 0.5 g L^{-1} after 5 h, showing aragonite spindle-shaped particles, (b) 0.5 g L^{-1} after 20 h, showing aragonite spindle-shaped particles with oriented surface overgrowths of calcite, (c) 1.0 g L^{-1} after 14 h, showing highly calcitic doughnut-shaped particles, and (d) 1.0 g L^{-1} after 7 days, showing calcite-overgrown particles along with thin vaterite plates.

Incorporation of relatively low concentrations of polyphosphate (0.1−0.5 g L^{-1}) in carbonate-containing microemulsions had negligible effect on the morphology and structure of the $CaCO_3$ precipitates produced on mixing with $Ca(AOT)_2$ reverse micelles. The particles were doughnut- or spindle-shaped with platelike aragonitic textures that transformed with time into striated patterns due to calcitic overgrowth (Figure 5a,b). PXRD analysis indicated that aragonite was the main polymorph formed after 24 h at a polyphosphate concentration of 0.1 g L^{-1}, whereas increasing amounts of calcite (typical d spacings: 0.303 (104), 0.249 (110), 0.211 (202), 0.188 (116)) were produced at 24 h when the additive concentration was increased to 0.5 g L^{-1} (Figure 2b,c).

Addition of higher concentrations of polyphosphate to carbonate-containing NaAOT microemulsions gave rise to significant changes in particle morphology and polymorphic structure. Crystallization of aragonite was progressively inhibited with the consequence that calcite was the main polymorph produced after 24 h at polyphosphate concentrations of 1 g L^{-1} (Figure 2d). At 2 g L^{-1}, PXRD profiles did not show any aragonite reflections; instead, peaks for vaterite were observed along with those for calcite (Figure 2e). SEM

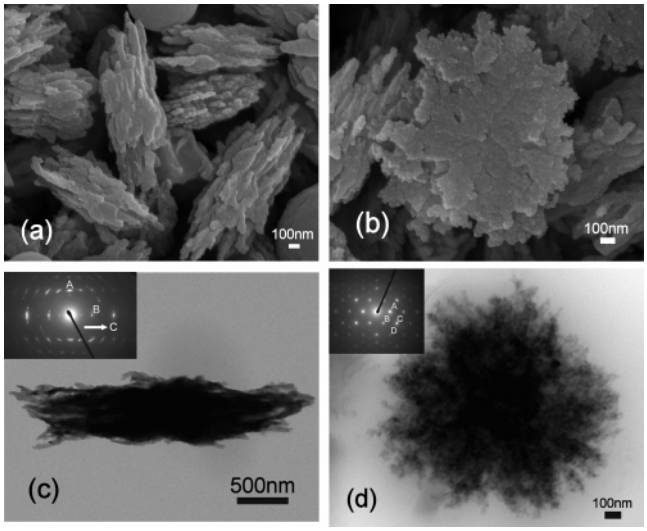

Figure 6. (a, b) SEM images of calcium carbonate particles produced at 2 g L^{-1} polyphosphate after 24 h; (a) bundles of filamentous particles, and (b) thin irregular plate viewed from above. (c) Corresponding TEM images and single-crystal electron diffraction pattern (inset) for an individual bundle formed after 7 days; the crystal is viewed along the [1$\bar{1}$0] zone and shows co-alignment of the crystallographic *c* axis and direction of filament growth (arrow; reflections, A = (110) and B = (006)). (d) Single-crystal vaterite plate formed after 24 h and viewed along the [001] crystallographic zone (reflections, A = ($\bar{1}$20), B = (110), C = (030), and D = (220)).

images showed the presence of doughnut-shaped aragonite particles in samples prepared within 14 h at 1 g L^{-1} polyphosphate that did not develop into spindle-shaped superstructures but became highly decorated with calcitic overgrowths elongated along the crystallographic *c* axis (Figure 5c). Samples collected after several days showed progressively increasing amounts of discrete irregular micrometer-sized plates along with calcite-overgrown aragonite particles (Figure 5d).

Increasing amounts of platelike particles were observed at 2 g L^{-1} polyphosphate, but no calcite/aragonite doughnut-shaped particles were produced. Instead, bundles of irregularly shaped filamentous crystals, approximately 1 μm in length, were observed in significant amounts within 24 h (Figure 6a,b). No structural or morphological changes were determined for the bundled or platelike particles over 7 days. In each case, EDX analysis of individual particles showed peaks for Ca (3.7, 4.0 keV), S (2.3 keV), P (2.0 keV), and Na (1.0 keV), indicating that AOT and polyphosphate ions were strongly associated with the particles even after extensive washing. TEM and electron diffraction studies confirmed that the individual bundles consisted of single crystals of calcite preferentially extended along the crystallographic *c* axis (Figure 6c) and that the platelike particles were single crystals of vaterite with the [001] direction aligned perpendicular to the plate surface (Figure 6d). The calcite electron diffraction patterns in particular often showed arced reflections indicative of highly textured single crystals with extensive morphological disorder. In contrast, the vaterite electron diffraction patterns generally comprised sharp spots implying a high degree of crystallographic coherence even though morphologically the crystal plates appeared to consist of multiple domains of irregularly shaped aggregates.

The results were consistent with a significant change in the growth mechanisms in the presence of entrapped polyphosphate. Without polyphosphate, formation of the doughnut-shaped aragonite superstructures occurs via the coordinated transformation and crystallization of colloidal aggregates of loosely packed surfactant-coated amorphous calcium carbonate nanoparticles, similar to previous investigations.[13] In contrast, formation of the filamentous calcite and platelike vaterite particles in the presence of polyphosphate curtails emergent behavior and reduces the system to a more conventional crystallization process, albeit one that is severely modified by the soluble additive. Calcite nucleation, both direct from solution or on aragonitic precursor particles, would be promoted under conditions of low supersaturation, which is consistent with polyphosphate-induced complexation of Ca^{2+} ions trapped in the water droplets. Indeed, control experiments in aqueous (nonmicroemulsion) solutions indicated that commensurate concentrations of polyphosphate resulted in significant levels of complexation along with calcium polyphosphate precipitation. On the other hand, the formation of increasing amounts of vaterite in the microemulsion system at higher additive concentrations suggests a specific influence of the encapsulated polyphosphate both on nucleation and subsequent formation of the platelike vaterite crystals. In particular, the (001) faces of vaterite appear to be highly stabilized in the presence of polyphosphate, possibly due to electrostatic and stereochemical complementarity at the crystal/additive interface.

Conclusions

The above results demonstrate that the encapsulation of a crystallization additive (sodium polyphosphate) into microemulsion water droplets can be used to influence nucleation and growth processes of calcium carbonate over a range of length scales. In the absence of polyphosphate, micrometer-sized doughnut-shaped particles consisting of densely packed layers of oriented platelike aragonite crystals are formed by controlled aggregation of surfactant-coated amorphous calcium carbonate primary particles. With time these superstructures progressively in-fill to produce polycrystalline multilayered spindle-shaped particles that become decorated with epitaxially oriented calcite nanofilament ougtrowths. In contrast, encapsulation of polyphosphate at concentrations exceeding 1 g L^{-1} inhibits aragonite crystallization, with the consequence that single crystals of filamentous calcite elongated along the [001] axis, along with increasing amounts of platelike vaterite single crystals with roughened (001) faces, are produced. Polyphosphate ions are strongly associated with the crystals, suggesting that the crystallization process is strongly influenced by changes in the level of supersaturation (polyphosphate-induced Ca^{2+} complexation) and by surface adsorption of the additive particularly on the vaterite (001) crystal face. The results suggest that entrapment of additives such as polyphosphate in the water droplets of reverse microemulsions could be of general interest as a novel approach in crystal science.

Acknowledgment. The authors thank EPSRC and the University of Bristol for financial support. S.T. thanks the Royal Thai Government for support of a leave of absence.

CM060847F